

# Effects of temperature on Rb and $^{129}\text{Xe}$ spin polarization in a nuclear magnetic resonance gyroscope with low pump power

Cite as: AIP Advances 7, 115101 (2017); <https://doi.org/10.1063/1.5000530>

Submitted: 16 August 2017 • Accepted: 15 October 2017 • Published Online: 01 November 2017

 Linlin Chen, Binqun Zhou, Guanqun Lei, et al.



View Online



Export Citation



CrossMark

## ARTICLES YOU MAY BE INTERESTED IN

### Chip-scale atomic devices

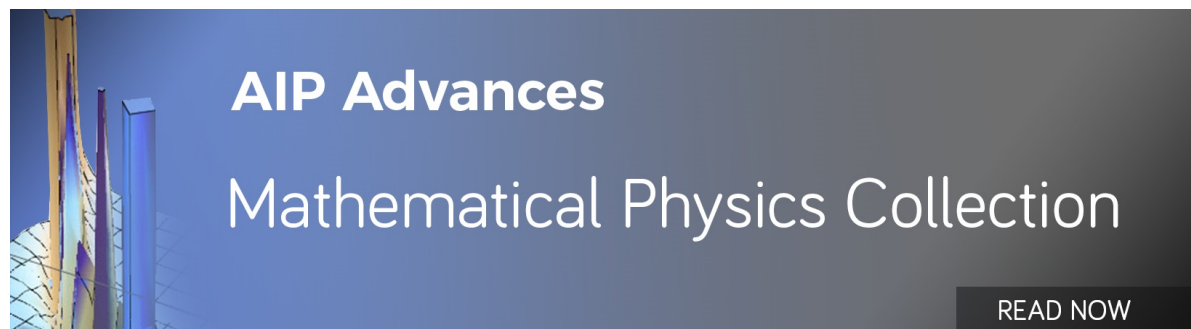
Applied Physics Reviews 5, 031302 (2018); <https://doi.org/10.1063/1.5026238>

### Measuring the spin polarization of alkali-metal atoms using nuclear magnetic resonance frequency shifts of noble gases

AIP Advances 5, 107119 (2015); <https://doi.org/10.1063/1.4932131>

### A parametrically modulated dual-axis atomic spin gyroscope

Applied Physics Letters 112, 054103 (2018); <https://doi.org/10.1063/1.5018015>



AIP Advances  
Mathematical Physics Collection

READ NOW

## Effects of temperature on Rb and $^{129}\text{Xe}$ spin polarization in a nuclear magnetic resonance gyroscope with low pump power

Linlin Chen, Binqun Zhou,<sup>a</sup> Guanqun Lei, Wenfeng Wu, Yueyang Zhai, Zhuo Wang, and Jiancheng Fang  
*School of Instrumentation Science and Opto-Electronics Engineering, Beihang University, Beijing 100191, China*

(Received 16 August 2017; accepted 15 October 2017; published online 1 November 2017)

We propose an average Rb polarization model to analyze the influence of temperature on the spin polarization of Rb and  $^{129}\text{Xe}$  in a Nuclear Magnetic Resonance Gyroscope (NMRG) with low pump power. This model is essentially based on summing the Rb spin polarization along the direction of the pump beam and dividing the result by the cell length. We experimentally study the spin polarization of Rb and  $^{129}\text{Xe}$  atoms as a function of the cell temperature at low values of the pump power. The experimental results and the values calculated with the average Rb polarization model are in good agreement for both Rb and  $^{129}\text{Xe}$ . The spin polarization of Rb atoms decreases with increasing cell temperature, with a decreasing trend which is rapid at temperatures below 110 °C, and slower at temperatures above 110 °C. The experimental values of the  $^{129}\text{Xe}$  polarization, obtained with a pump power of 1 mW, first increase to a maximum  $P_{^{129}\text{Xe-ave}} = 0.66\%$  at 118 °C, and then decreases as the temperature increases. Increasing the power of the pump beam shifts the temperature maximum to a higher value. Our model is suitable for the analysis of Rb and  $^{129}\text{Xe}$  polarization at high temperature and low pump power, i.e. when the power of the pump beam is completely absorbed within a few millimeters of the front window of the cell. Therefore, the present model can provide theoretical support for the improvement of the Signal-to-Noise-Ratio (SNR) of the NMRG, and to determine its optimal working temperature. © 2017 Author(s). All article content, except where otherwise noted, is licensed under a Creative Commons Attribution (CC BY) license (<http://creativecommons.org/licenses/by/4.0/>). <https://doi.org/10.1063/1.5000530>

### I. INTRODUCTION

The Nuclear Magnetic Resonance Gyroscope (NMRG) is a rotation-speed sensor, which detects the angular rate by measuring a shift in the Larmor precession frequency of nuclear spins in an applied magnetic field.<sup>1</sup> The NMRG itself is inherently immune to vibration, and has no moving parts.<sup>2,3</sup> Moreover, such a measurement system can outperform other types of gyros for small, low-power applications.<sup>4</sup> The Northrop Grumman Corporation (NGC) uses a vertical cavity surface-emitting laser (VCSEL) to optically pump the alkali metal atoms, with an output laser power of the VCSEL below 2 mW. The spin polarization of alkali metal atoms and noble gases influence the magnetometer sensitivity and the SNR of the NMRG. Therefore, the spin polarization of the alkali atoms and noble gases in low pump power conditions should be optimized in order to increase the magnetometer sensitivity and the SNR of the NMRG.

Polarized alkali metal atoms and hyperpolarized noble gases can be used in many applications, including Magnetic Resonance Imaging (MRI),<sup>5,6</sup> optical atomic magnetometers,<sup>7-9</sup> and spin-precession gyroscopes.<sup>2,4</sup> The optimization of the Spin-Exchange Optical Pumping (SEOP)

---

<sup>a</sup>bqzhou@buaa.edu.cn

parameters, temperature and gas flow rate through the cell, has been carried out for MRI in the case of high pumping power (above 60 W), low-pressure,<sup>10</sup> and high-pressure.<sup>11,13</sup> The dependence of the magnetometer sensitivity on the cell temperature and the pump beam power has been investigated by John Kitching *et al.*,<sup>8</sup> Testo Kobayashi *et al.*,<sup>7,14</sup> and M.V. Romalis *et al.*<sup>9</sup> However, the working conditions of MRI and optical magnetometers are not suitable for the NMRG. The optimization of the parameters of NMRGs based on  $^{133}\text{Cs}$ - $^{129}\text{Xe}/^{131}\text{Xe}$  has been analyzed at a fixed temperature of 110 °C.<sup>15</sup> However, the effects of temperature on the spin polarization of Rb and  $^{129}\text{Xe}$  in a low pump power of the NMRG have not been studied yet to the best of our knowledge.

In this work, we present an average Rb polarization model to analyze the effects of temperature on the spin polarization of Rb and  $^{129}\text{Xe}$  in a NMRG with a low pump power. The optical depth is measured as a function of the frequency near the Rb atoms D1 line in order to calculate the number density of Rb atoms and the buffer gas pressure. The Rb spin polarization is then simulated numerically along the direction of the pump beam, as a function of temperature and of the transmission distance in the cell. The Rb polarization is experimentally measured at different temperatures, finding good agreement with the theoretical calculations based on our average Rb polarization model. The  $^{129}\text{Xe}$  spin polarization is also measured as a function of temperature at different pump powers. The experimental results are in good agreement with the calculated values, based on the average Rb polarization model, in this case as well. Therefore, the present model can provide theoretical support for the improvement of the SNR of the NMRG.

## II. PRINCIPLE

The basic principle of the NMRG is depicted in FIG. 1. A square glass cell contains Rb and  $^{129}\text{Xe}$ ,  $\text{N}_2$  as quenching gas, and  $^4\text{He}$  as buffer gas. A circularly polarized pump beam propagates parallel to a static magnetic field  $B_0$ , along the z axis, in order to optically pump the Rb atoms. Through spin-exchange collisions with polarized Rb atoms, the net magnetization of the polarized  $^{129}\text{Xe}$  nuclei becomes aligned along the z axis. An oscillating magnetic field  $B_1$  is then applied along the x axis in order to stimulate the  $^{129}\text{Xe}$  nuclei precession, which is detected by the *in situ* Rb magnetometer. As the on-resonant pump beam propagates through the vapor cell, it is absorbed (partially or completely) by the alkali vapor. Therefore, the analytical expression for the position-dependent optical pumping rate  $R_{\text{op}}(z)$  within the cell can be expressed as follows<sup>16</sup>

$$dR_{\text{op}}(z) = -n_{\text{Rb}}\sigma(\nu) \left( 1 - \frac{R_{\text{op}}(z)}{R_{\text{op}}(z) + R_{\text{sd}}} \right) R_{\text{op}}(z) dz, \quad (1)$$

where  $n_{\text{Rb}}$  is the number density of Rb atoms,  $\sigma(\nu)$  is the optical absorption cross section,  $R_{\text{op}}$  is the optical pumping rate, and  $R_{\text{sd}}$  is the Rb spin destruction rate. The  $^{87}\text{Rb}$  D1 line contains four

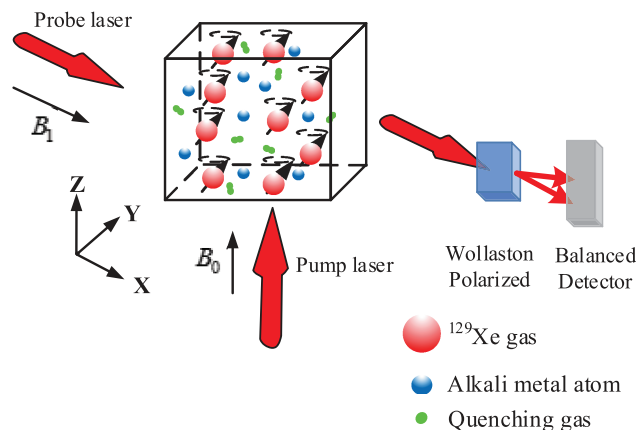


FIG. 1. Basic elements of the experimental setup of NMRG.

hyperfine transitions. The total optical absorption cross section at frequency  $\nu$  is given by

$$\sigma(\nu) = \pi r_e c f \sum_{FF'} \frac{(2F+1)(2F'+1)}{2I+1} \left\{ \begin{matrix} J & J' & 1 \\ F & F' & I \end{matrix} \right\}^2 \text{Re}[V(\nu - \nu_{FF'})], \quad (2)$$

where  $r_e = 2.82 \times 10^{-15}$  m is the classical electron radius,  $c = 3 \times 10^8$  m/s is the speed of light,  $f = 1/3$  is the oscillator strength,  $F = 1, 2$  and  $F' = 1, 2$  are two hyperfine sublevels for  $5S_{1/2}$  and  $5P_{1/2}$  terms respectively.  $J$  and  $J'$  are the quantum numbers of electronic angular momentum for ground and first excited states respectively, and the Voigt profile  $V(\nu - \nu_{FF'})$  is the atomic frequency response to light due to natural lifetime, pressure broadening, and Doppler broadening, which can be expressed by

$$V(\nu - \nu_0) = \frac{2\sqrt{\ln 2/\pi}}{\Gamma_G} \omega \left\{ \frac{2\sqrt{\ln 2} [(\nu - \nu_0) + i\Gamma_L/2]}{\Gamma_G} \right\} \quad (3)$$

where  $\Gamma_L$  is the Lorentzian broadening which is the sum of natural and pressure broadening,  $\Gamma_G$  is the Doppler broadening,  $\nu$  is the light frequency,  $\nu_0$  is the resonance frequency of each transition,  $\omega(x) = e^{-x^2} [1 - \text{erf}(-ix)]$  is the complex error function.

The solution to Eq. (1) is the principal value of the Lambert W-function, which is given by

$$R_{\text{op}}(z) = R_{\text{sd}} W \left[ \frac{R_{\text{op}}(0)}{R_{\text{sd}}} \exp \left( \frac{R_{\text{op}}(0)}{R_{\text{sd}}} - n_{\text{Rb}} \sigma(\nu) z \right) \right], \quad (4)$$

where  $R_{\text{op}}(0)$  is the optical pumping rate at the entrance window of the vapor cell. Several causes may lead to Rb depolarization: wall collisions, radiation trapping, interactions between Rb atoms or between Rb and  $\text{N}_2$ ,  $^4\text{He}$ , and  $^{129}\text{Xe}$ , which can be summarized in the following equation<sup>17,18</sup>

$$R_{\text{sd}} = R_{\text{sd}}^{\text{BC}} + R_{\text{sd}}^{\text{vdW}} + R_{\text{se}}^{\text{Rb-}^{129}\text{Xe}} + R_{\text{D}} + R_{\text{m}} + R_{\text{rt}}, \quad (5)$$

where  $R_{\text{sd}}^{\text{BC}}$  is the binary spin destruction rate,  $R_{\text{sd}}^{\text{vdW}}$  is the three-body spin destruction rate,  $R_{\text{se}}^{\text{Rb-}^{129}\text{Xe}}$  is the Rb- $^{129}\text{Xe}$  spin-exchange rate,  $R_{\text{D}}$  indicates the rate of wall collisions,  $R_{\text{m}}$  is the pumping rate of the probe beam,  $R_{\text{rt}}$  is the spin-relaxation rate due to radiation trapping. Thus, the overall spin destruction rate as a result of binary collisions for an optical pumping mixture containing  $\text{N}_2$ ,  $^4\text{He}$ , and  $^{129}\text{Xe}$  can be written as

$$R_{\text{sd}}^{\text{BC}} = \sum_i n_i \kappa_{\text{sd}}^{\text{Rb-i}}, \quad (6)$$

where  $n_i$  indicates the number density of each gas in the cell,  $\kappa_{\text{sd}}^{\text{Rb-i}}$  indicates the spin destruction coefficients for the binary collisions between Rb atoms and the atoms of each gas, which have been measured as a function of temperature, finding  $4.2 \times 10^{-13} \text{ cm}^3 \text{ s}^{-1}$ ,<sup>19</sup>  $1 \times 10^{-29} T^{4.26} \text{ cm}^3 \text{ s}^{-1}$ ,<sup>19</sup>  $1.3 \times 10^{-25} T^3 \text{ cm}^3 \text{ s}^{-1}$ ,<sup>20</sup> and  $6.3 \times 10^{-17} (T - 273.15)^{1.17} \text{ cm}^3 \text{ s}^{-1}$  for Rb,  $^4\text{He}$ ,  $\text{N}_2$ ,  $^{129}\text{Xe}$ ,<sup>21</sup> respectively, where  $T$  is the temperature in K. The Rb spin destruction rate caused by the formation of Rb- $^{129}\text{Xe}$  van der Waals molecules at low pressure can be expressed as<sup>22</sup>

$$R_{\text{sd}}^{\text{vdW}} = \left( \frac{66183}{1 + 0.92 \frac{n_{\text{N}_2}}{n_{^{129}\text{Xe}}} + 0.31 \frac{n_{^4\text{He}}}{n_{^{129}\text{Xe}}}} \right) \left( \frac{T}{423} \right)^{-2.5}. \quad (7)$$

The rate of diffusion of Rb atoms to the walls is described by<sup>17</sup>

$$R_{\text{D}} = 0.5 \text{ cm}^2 \left( \frac{\sqrt{1 + T/(273.15\text{K})}}{p_{^4\text{He}}/(1\text{amg})} \right) \left( \frac{\pi}{L/2} \right)^2, \quad (8)$$

where  $L$  is the length of the cubic vapor cell, and  $p_{^4\text{He}}$  is the  $^4\text{He}$  pressure. In our actual experiments, the probe laser frequency is significantly detuned from the D1 transition line of Rb atoms, and the laser power is generally low. Therefore, the probe laser pumping term  $R_{\text{m}}$  can be ignored. The spin destruction rate contribution from radiation trapping can be described by the following equation<sup>23</sup>

$$R_{\text{rt}} = K(M - 1)QR_{\text{op}}, \quad (9)$$

where  $K$  describes the degree of depolarization caused by a resorbed photon,  $M$  is the average number of times that a photon is emitted before it leaves the vapor cell,  $Q = 1/(1 + p_{\text{N}_2}/p'_Q)$ , where  $p_{\text{N}_2}$  is the

$N_2$  pressure, and  $p'_Q$  is a characteristic pressure. For the D1 line of  $^{87}\text{Rb}$  at  $100^\circ\text{C}$ ,  $p'_Q$  is 3.9 Torr. Therefore, the position-dependent Rb spin polarization,  $P_{\text{Rb}}(z)$ , at a position  $z$  along the direction of the pump beam in the vapor cell can be written as<sup>16</sup>

$$P_{\text{Rb}}(z) = \frac{R_{\text{op}}(z)}{R_{\text{op}}(z) + R_{\text{sd}}}. \quad (10)$$

If the pump beam power at the entrance window is below 2 mW, the optical pumping rate is far lower than the Rb spin destruction rate. As the cell temperature increases, the pump beam can be completely absorbed within a few millimeters of the front window of the cell. Therefore, the spin polarization of Rb atoms drops to zero according to Eq. (10), and the *in situ* Rb atomic magnetometer can no longer work properly. However, in our actual experiments, the magnetic resonance signal of the Rb atoms and the Free Induction Decay (FID) signal of the  $^{129}\text{Xe}$  nuclei can still be acquired. The average Rb polarization model can thus be employed to analyze the spin polarization of Rb and  $^{129}\text{Xe}$  atoms, which can be estimated by summing the spin polarization  $P_{\text{Rb}}(z)$  along the  $z$  axis and dividing the result by the cell length. The average Rb polarization can thus be described by the following equation

$$P_{\text{Rb-ave}} = \frac{1}{L} \int_0^L \frac{R_{\text{op}}(z)}{R_{\text{op}}(z) + \Gamma_{\text{sd}}} dz. \quad (11)$$

The average  $^{129}\text{Xe}$  nuclear spin polarization can be given by<sup>11</sup>

$$P_{^{129}\text{Xe-ave}} = \frac{\gamma_{\text{SE}}}{\gamma_{\text{SE}} + \Gamma_{\text{Xe}}} P_{\text{Rb-ave}}, \quad (12)$$

where  $\gamma_{\text{SE}}$  is the  $^{129}\text{Xe}$ -Rb spin-exchange rate, and  $\Gamma_{\text{Xe}}$  is the  $^{129}\text{Xe}$  nuclear spin destruction rate, which is mainly governed by the rate of wall collisions. Therefore, the wall collisions relaxation rate can be expressed by<sup>12</sup>

$$\Gamma_{\text{Xe}} = \left( \frac{S}{V} \right) \frac{\bar{V}_{^{129}\text{Xe}}}{2} (\gamma \bar{H}_l \tau_s^o)^2 e^{\frac{2E}{k_B T}}, \quad (13)$$

where  $S/V$  is the microscopic wall surface to volume ratio,  $\gamma$  is the gyromagnetic ratio of  $^{129}\text{Xe}$  nuclei,  $k_B$  is the Boltzman constant,  $\bar{H}_l$  is the effective local magnetic dipolar field at the wall surface,  $\tau_s^o$  is the high temperature sticking time which is on the order of  $10^{-13}$  s,  $E$  is the adsorption energy,  $\bar{V}_{^{129}\text{Xe}} = \sqrt{\frac{8k_B T}{\pi M}}$  is the  $^{129}\text{Xe}$  velocity, which is proportional to  $\sqrt{T}$ . Therefore, the wall collisions relaxation rate  $\Gamma_{\text{Xe}}$  is proportional to  $\sqrt{T} e^{\frac{2E}{k_B T}}$ . The  $^{129}\text{Xe}$ -Rb spin-exchange rate is dominated by binary collisions and three-body complex formations. An analytical expression of the term  $\gamma_{\text{SE}}$  can be given by<sup>25</sup>

$$\gamma_{\text{SE}} = \left( \langle \sigma v \rangle + \frac{\kappa_{\text{SE}, ^4\text{He}}}{n_{^4\text{He}}} + \frac{\kappa_{\text{SE}, ^{129}\text{Xe}}}{n_{^{129}\text{Xe}} \left( 1 + 0.275 \frac{n_{N_2}}{n_{^{129}\text{Xe}}} \right)} \right) n_{\text{Rb}}, \quad (14)$$

where  $\langle \sigma v \rangle$  is the binary collisions spin-exchange cross section of Rb and  $^{129}\text{Xe}$ , which has been measured to be  $\langle \sigma v \rangle = 2.17 \times 10^{-16} \text{ cm}^3 \text{ s}^{-1}$ .  $\kappa_{\text{SE}, ^4\text{He}}$  and  $\kappa_{\text{SE}, ^{129}\text{Xe}}$  respectively indicate the van der Waals specific spin-exchange rates for  $^4\text{He}$  and  $^{129}\text{Xe}$ , which have been estimated by G.D.Gates<sup>25</sup> to be  $\kappa_{\text{SE}, ^4\text{He}} = 1.7 \times 10^4 \text{ s}^{-1}$  and  $\kappa_{\text{SE}, ^{129}\text{Xe}} = 5.23 \times 10^3 \text{ s}^{-1}$ . The spin-exchange rate experienced by Rb atoms is  $R_{\text{se}}^{\text{Rb-}^{129}\text{Xe}} = \frac{n_{^{129}\text{Xe}}}{n_{\text{Rb}}} \gamma_{\text{SE}}$ . Therefore, based on Eq.(13) and Eq.(14), the transverse spin relaxation rate of  $^{129}\text{Xe}$  nuclei can be expressed by

$$\frac{1}{T_2} = C_1 n_{\text{Rb}} + C_2 \sqrt{T} e^{\frac{2E}{k_B T}} + C_3; \quad (15)$$

where  $C_i$  ( $i=1,2,3$ ) is a constant coefficient, which are independent of the cell temperatures. In summary, the Rb polarization and  $^{129}\text{Xe}$  polarization are influenced by temperature, pump power,  $N_2$  pressure, and  $^{129}\text{Xe}$  pressure based on Eq.(11) and Eq.(12).

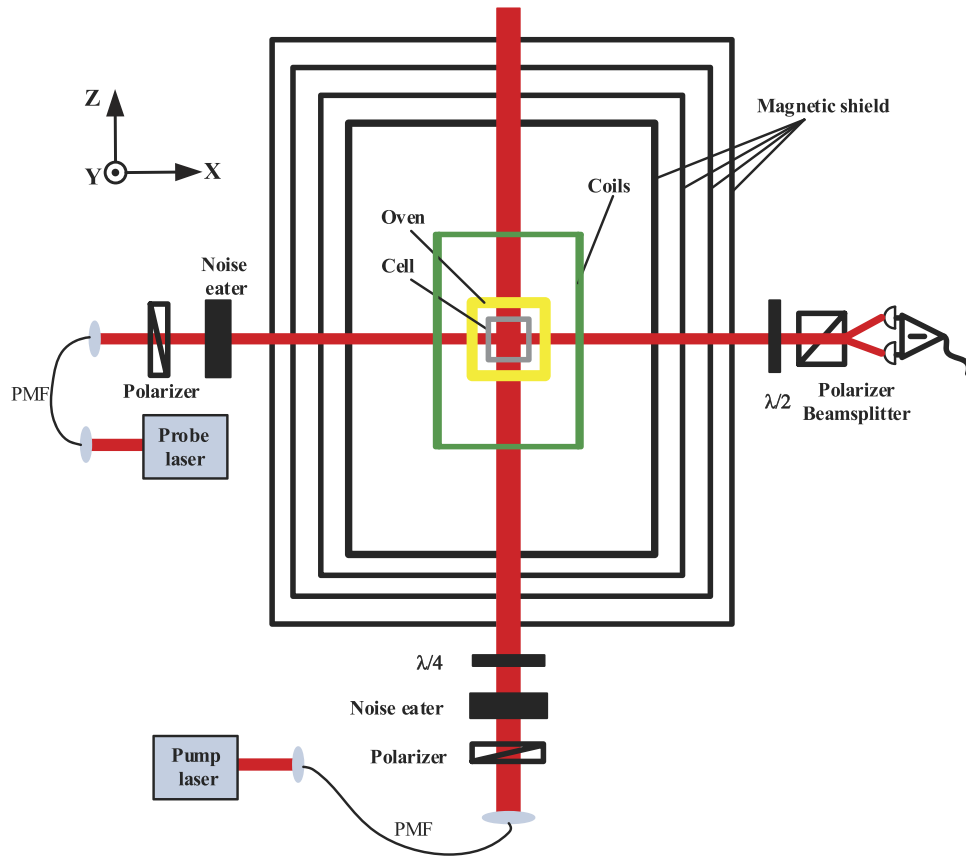


FIG. 2. Experimental setup of the NMRG. The circularly polarized pump beam and the linearly polarized probe beam propagate along the  $z$  and  $x$  directions, respectively.

### III. EXPERIMENTAL SETUP

The experimental setup is shown in FIG.2. A cubic vapor cell, with an inner length of 3 mm, containing a droplet of Rb metal. Unless the parameters are varied, the vapor cell is filled with about 5 Torr of  $^{129}\text{Xe}$ , 10 Torr of  $\text{N}_2$  as quenching gas, and 200 Torr of  $^4\text{He}$  as buffer gas. The vapor cell is placed into an oven, heated to  $100^\circ\text{C}$  by an electronic heater.

A four-layer cylindrical magnetic shield is employed to reduce the external magnetic field. The residual magnetic field can be compensated actively by the triaxial coil inside the magnetic shields.

The circularly polarized pump beam, propagating along the  $z$  axis, is generated from a Photodigm DBR laser, which is tuned to the D1 transition line of Rb atoms. The pump power is about 1 mW. The linearly polarized probe beam, emitted by another Photodigm DBR laser, is detuned by about 50 GHz from the D1 transition line of Rb atoms in order to detect the magnetometer signal, which is perpendicular to the pump beam at the center of the cell. The output signal of the NMRG, demodulated by a lock-in amplifier, is acquired using a Model 2307 and a NI PXI-4461 DAQ card with a sampling rate of 10 KHz.

### IV. EXPERIMENTAL RESULTS AND DISCUSSION

In the experiment, a static magnetic field of amplitude  $B_0 = 10\mu\text{T}$  is applied along the  $z$  axis as described in the previous section. A resonant magnetic field of the form  $B_1(t) = B_1 \cos(\omega t)$ , oscillating at the Larmor precession frequency of the  $^{129}\text{Xe}$  nuclei, is applied along the  $x$  axis. The power of the probe beam is low enough (about 0.3 mW) to reduce unwanted laser-induced spin polarization effects on Rb atoms. The absorption of the linearly polarized D1 probe beam is described by an exponential

law of the form<sup>16</sup>

$$I_0 = I_i \exp(-n\sigma(\nu)L), \quad (16)$$

where  $I_i$  and  $I_0$  indicate the power of the probe beam before and after the cell, respectively. Assuming the temperature is 100 °C and the central frequency is 377107.46 GHz, we can calculate the profile of absorption cross section with buffer pressure of 200 Torr based on Eq.(2), which is shown in Fig.3 (a). The hyperfine structure is clearly resolved. The optical depth OD can be defined as  $OD=n\sigma(\nu)L$ . The optical depth as a function of the frequency deviation from the center frequency is shown in Fig.3 (b), the total absorption profile is a “M” type, which is agree with the theoretical curve very well. In the center of the D1 line, the absorption is so strong that the corresponding optical depth cannot be measured accurately and is therefore ignored. When  $n_{Rb}$  is about  $4.58 \times 10^{12} \text{ cm}^{-3}$  and  $\Gamma$  is about 4.64 GHz, the fitting result and the measured data show good agreement. Since the value of  $\Gamma$  calculated considering the pressure of the buffer gases is 4.98 GHz, the fitting result can be considered be accurate. The value of  $n_{Rb}$  calculated at the operating temperature is  $6.02 \times 10^{12} \text{ cm}^{-3}$ . The measured  $n_{Rb}$  value is about by 0.24 times smaller than those expected at the operating temperature.

FIG.4 displays a contour plot of Rb spin polarization as a function of the cell temperature and the transmission distance along the z axis, as described by Eq. (10). The optical pump rate at the pump

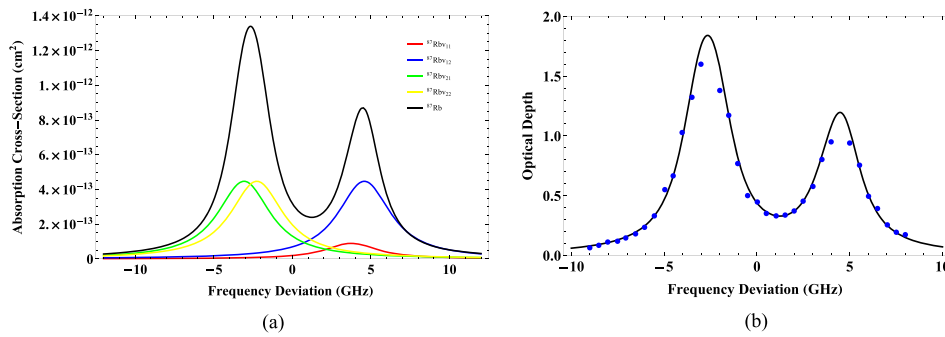


FIG. 3. (a) The absorption profile of  $^{87}\text{Rb}$  as a function of frequency deviation based on Eq.(2) at temperature of 100 °C. (b) The optical depth of the linearly polarized D1 probe beam propagating through a cell with 3 mm internal length at 100 °C. The wavelength interval is 0.001 nm (corresponding to 0.5 GHz). The atomic number density of Rb ( $n_{Rb}$ ) is estimated to be about  $4.58 \times 10^{12} \text{ cm}^{-3}$ , and the linewidth of pressure-broadened optical absorption  $\Gamma$  is about 4.64 GHz.

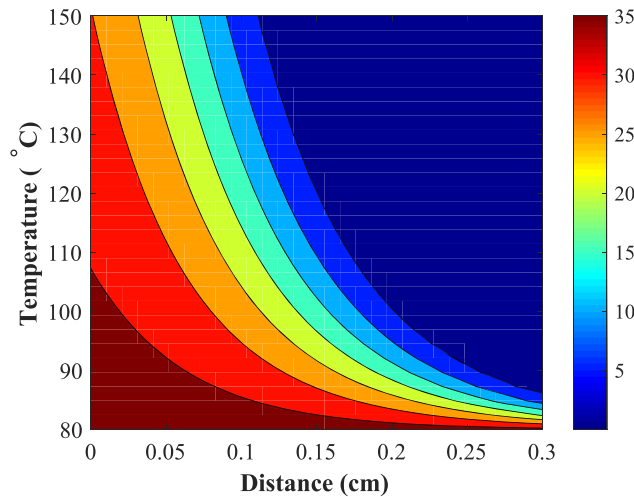


FIG. 4. The spin polarization of Rb atoms as a function of the cell temperature and the position along the z axis expressed by Eq. (10) at the pump power of 1 mW. The color scale encodes the spin polarization of Rb atoms in percentage.

power of 1 mW is far lower than the Rb spin destruction rate. Therefore, a large polarization gradient can be obtained along the  $z$  axis. At a temperature of 130 °C, the spin polarization of Rb decreases from  $P_{Rb} = 35\%$  at the entrance window to zero at the center of the vapor cell, which means that all the pump beam is completely absorbed over this distance. Thus, the position-dependent Rb polarization model is not suitable for analyzing the effects of temperature on Rb and  $^{129}\text{Xe}$  spin polarization in a NMRG with low pump power. Therefore, the Rb spin polarization should be evaluated by using the average Rb polarization model.

We measure the Rb polarization as a function of temperature (a), pump power (b), and  $N_2$  pressure (c). We compare these experimental results to our average Rb polarization model based on Eq. (11), which is shown in FIG.5. The experimental results of the Rb polarization are measured by detecting the NMR frequency shifts of the  $^{129}\text{Xe}$  nuclei.<sup>24</sup> The trends in the average Rb polarization model and the experimental results agree well for parameters. In FIG.5 (a), the temperature dependence of Rb polarization is measured by using both a 1 mW and a 2 mW pump beam. The spin polarization of Rb atoms decreases with the increasing cell temperature. Its decreasing trend is rapid below 110 °C, and slower above 110 °C. This indicates that the power of the pump beam is almost completely absorbed within a few millimeters of the front window of the cell. In FIG.5 (b), when the incident pump power is below 0.6 mW, the Rb polarization increases sharply with the increasing pump power. On the other hand, when the incident pump power is over 0.6 mW, the Rb polarization increases gradually with the increasing pump power. This indicates that the Rb atoms become nearly fully polarized throughout the cell at higher pump power. In FIG.5 (c), the figure indicates that the Rb polarization will keep growing until saturation as the  $N_2$  pressure increases with  $M$  around 28 and  $K$  around 0.12.

The transverse relaxation time of  $^{129}\text{Xe}$  is measured by using the Free Induction Decay (FID) method. We use a  $\pi/2$  pulse to drive up the  $^{129}\text{Xe}$  precession and then allow the coherence to decay naturally. We can fit the decaying curve to a simple exponential curve  $V = V_0 e^{-T/\tau}$ , and extract the

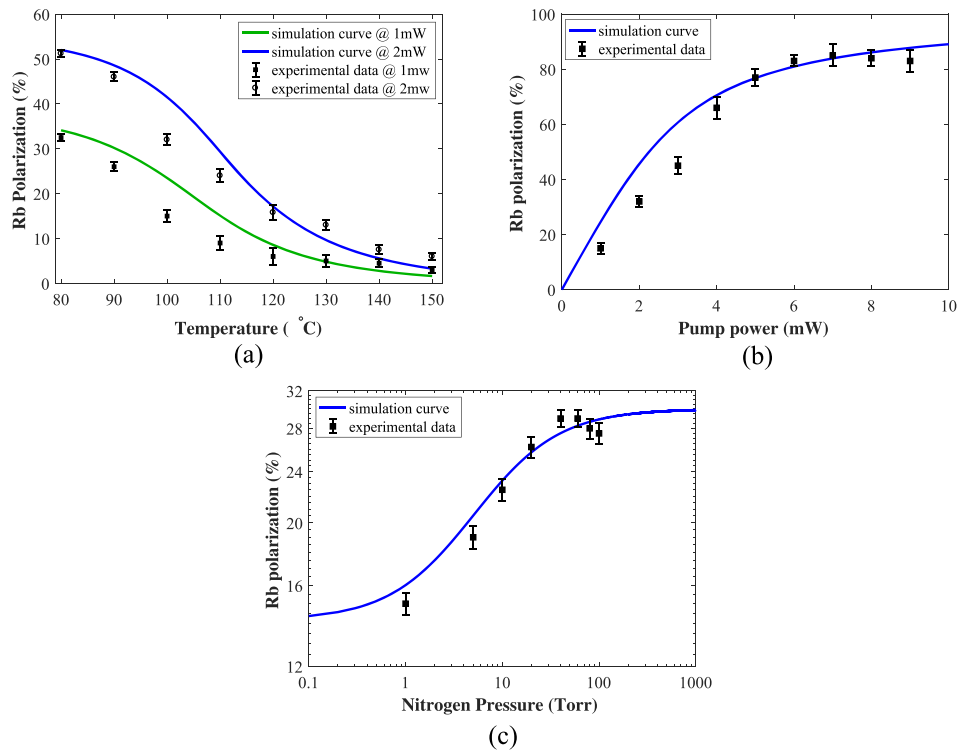


FIG. 5. Comparison of the experimental data to our numerical model for Rb polarization. The varied parameters are: (a) cell temperature, (b) pump power, (c)  $N_2$  pressure ( $K = 0.12$ ,  $M = 28$ ). The experimental data are in reasonable agreement with the model based on Eq.(11).



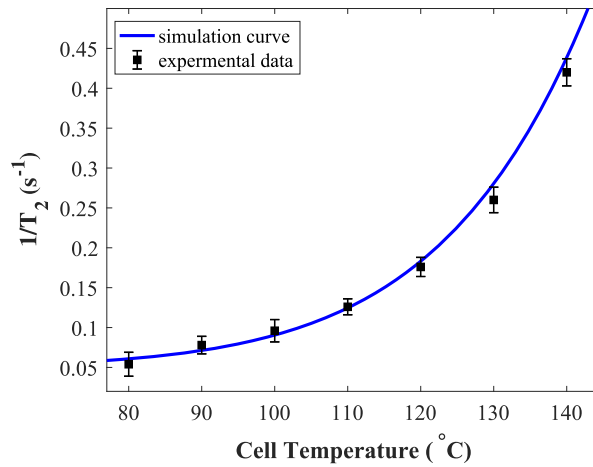


FIG. 6. The transverse spin relaxation rate of  $^{129}\text{Xe}$  as a function of temperatures. The fit based on Eq.(15) gives the adsorption energy  $E = 0.044$  eV, and the temperature independent wall collision relaxation rate coefficient  $C_2 = 3.9 \times 10^{-6} \text{s}^{-1} \text{o}^{-1/2}$ .

transverse relaxation time from the fit solution. Fig. 6 shows the transverse relaxation rate as a function of temperatures. Overlaying the data is a fit based on Eq.(15). We can obtain the adsorption energy  $E=0.044$  eV, and the temperature independent wall collisions rate coefficient  $C_2 = 3.9 \times 10^{-6} \text{s}^{-1} \text{o}^{-1/2}$ . Therefore, the temperature dependent wall collisions influence the  $^{129}\text{Xe}$  polarization, which can be increased by using efficient cell wall coatings.

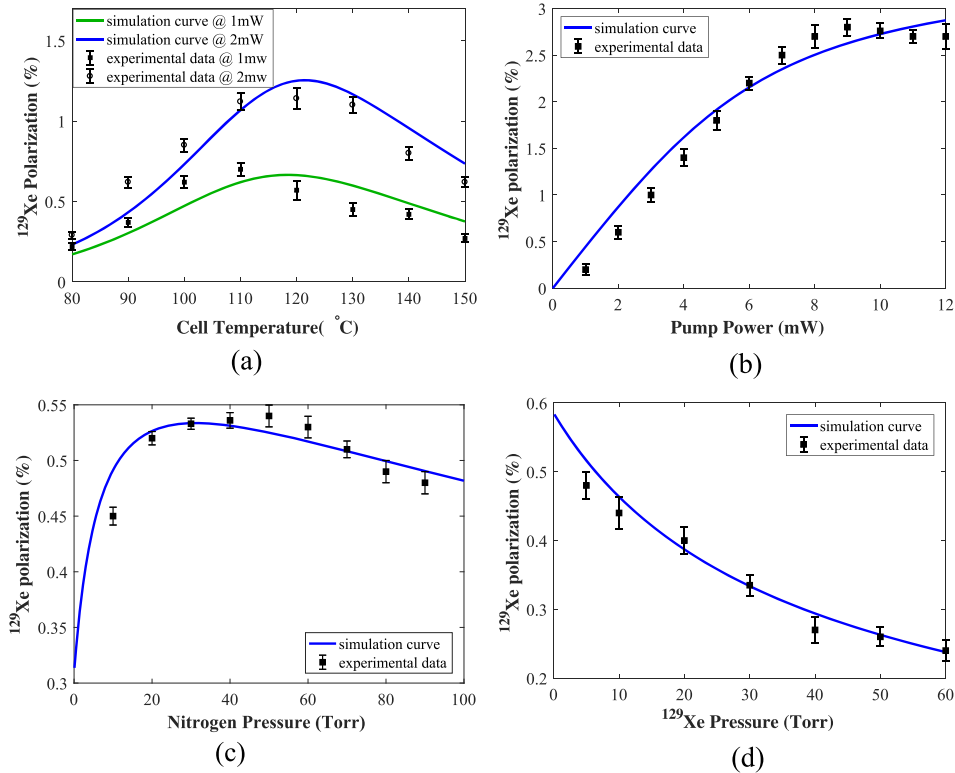


FIG. 7. Comparison of the experimental data on  $P_{129}\text{Xe}$  to our numerical model as a function of: (a) cell temperature, (b) pump power, (c)  $\text{N}_2$  pressure ( $K = 0.12$ ,  $M = 28$ ), (d)  $^{129}\text{Xe}$  pressure. The model curves indicate an adjustment of the spin-exchange rate by a factor of 0.75 to improve matching with the lower measured  $^{129}\text{Xe}$  polarization.

We measure the  $^{129}\text{Xe}$  polarization as a function of temperature (a), pump power (b),  $N_2$  pressure (c), and  $^{129}\text{Xe}$  pressure (d). We compare these experimental results to our model based on Eq. (11) and Eq. (12), which is shown in FIG.7. In FIG.7 (a), the calculations show that  $^{129}\text{Xe}$  polarization first increases to a maximum value of  $P_{^{129}\text{Xe-ave}} = 0.66\%$  at  $118\text{ }^\circ\text{C}$ , and then decreases as the temperature increases at a pump power of 1 mW. Increasing the power of the pump beam moves the temperature maximum upward. The temperature maximum shifts from  $118\text{ }^\circ\text{C}$  to  $121\text{ }^\circ\text{C}$  and the spin polarization of  $^{129}\text{Xe}$  increases by a factor of 2 in case of the higher-power pump beam. The differences between experimental results and calculated values are primarily due to discrepancies between the actual number density and the expected number density of each gas in the cell. Thus, the working temperature of the NMRG can be optimized in order to maximize the spin polarization of the  $^{129}\text{Xe}$  nuclei. In FIG.7 (b), the spin polarization of  $^{129}\text{Xe}$  nuclei first increases sharply below 6 mW and then increases gradually at higher pump powers. In FIG.7 (c), when the  $N_2$  pressure is below 20 Torr, the spin polarization of  $^{129}\text{Xe}$  nuclei increases sharply. Beyond this pressure, the spin polarization of  $^{129}\text{Xe}$  nuclei strongly decreases. This indicates that additional  $N_2$  pressure is necessary to maintain high polarization as the  $N_2$  increase, but an excessive amount leads to spin relaxation and limits the polarization that can be achieved. In FIG.7 (d), the figure indicates that the  $^{129}\text{Xe}$  polarization is decreased with increasing the  $^{129}\text{Xe}$  pressure. Therefore, in order to obtain higher  $^{129}\text{Xe}$  polarization with low pump power, the  $^{129}\text{Xe}$  pressure can't be too high.

## V. CONCLUSION

In this work, an average Rb polarization model is developed in order to analyze the influence of temperature on the spin polarization of Rb and  $^{129}\text{Xe}$  in a Nuclear Magnetic Resonance Gyroscope (NMRG) with low pump power. The experimental results in terms of Rb and  $^{129}\text{Xe}$  spin polarization are consistent with the theoretical calculations based on this average Rb polarization model. The advantage of this model lies in the possibility to analyze the temperature dependences of the spin polarization of Rb and  $^{129}\text{Xe}$  at low pump power, especially when the power is completely absorbed. Moreover, the calculations can provide the theoretical support for the experimental results, which can be useful to determine the optimal working temperature of the NMRG.

## ACKNOWLEDGMENTS

This research was supported by National High Technology Research and Development Program of China (2014AA123401); by the National Natural Science Foundation of China (NSFC) (61673041 and 61227902); by the Ministry of Science and Technology of the People's Republic of China (2016YFB0501601).

- <sup>1</sup> M. Larsen and M. Bulatowicz, *Proc. IEEE* **12**, 978 (2012).
- <sup>2</sup> D. Meyer and M. Larsen, *Gyroscope and Navigation* **5**(2), 75 (2014).
- <sup>3</sup> J. Kitching, S. Knappe, and E. A. Donley, *Proc. IEEE* **11**, 1748–1759 (2011).
- <sup>4</sup> T. G. Walker and M. Larsen, *Adv. At. Mol. Opt. Phys.* **65**, 373–401 (2016).
- <sup>5</sup> M. Rao, N. J. Stewart, G. Norquay, P. D. Griffiths, and J. M. Wild, *Magn. Reson. Med.* **75**, 2227–2234 (2016).
- <sup>6</sup> J. P. Mugler and T. A. Altes, *J. of Magn. Reson. Imaging* **37**, 313–331 (2013).
- <sup>7</sup> N. Mizutani, K. Okano, K. Ban, S. Ichihara, A. Terao, and T. Kobayashi, *AIP Advances* **4**, 057132 (2014).
- <sup>8</sup> R. Jiménez-Martínez, W. C. Griffith, S. Knappe, J. Kitching, and M. Prouty, *JOSA B* **29**, 3398–3403 (2012).
- <sup>9</sup> M. P. Ledbetter, I. M. Savukov, V. M. Acosta, and D. Budker, *Phys. Rev. A* **77**, 033408 (2008).
- <sup>10</sup> I. C. Ruset, S. Ketel, and F. W. Hersman, *Phys. Rev. Lett.* **96**, 053002 (2006).
- <sup>11</sup> B. Driehuys, G. D. Cates, E. Miron, D. K. Walter, and W. Happer, *Appl. Phys. Lett.* **69**, 1668–1670 (1996).
- <sup>12</sup> W. A. Fitzsimmons, L. L. Tankersley, and G. K. Walters, *Phys. Rev* **179**, 156 (1969).
- <sup>13</sup> A. L. Zook, B. B. Adhyaru, and C. R. Bowers, *J. Magn. Reson* **159**, 175–182 (2002).
- <sup>14</sup> K. Kamada, S. Taue, and T. Kobayashi, *Japanese Journal of Applied Physics* **50**, 056602 (2011).
- <sup>15</sup> D. W. Zhang, Z. Y. Xu, and M. Zhou, *Chinese Physics B* **26**, 023201 (2017).
- <sup>16</sup> S. J. Seltzer, Ph. D. thesis, University of Princeton, Princeton, 2008.
- <sup>17</sup> T. W. Kornack, Ph. D. thesis, University of Princeton, Princeton, 2005.
- <sup>18</sup> I. A. Nelson, Ph. D. thesis, University of Wisconsin-Madison, Wisconsin, 2001.
- <sup>19</sup> A. B. A. Baranga, S. Appelt, M. V. Romalis, C. J. Erickson, A. R. Young, G. D. Cates, and W. Happer, *Phys. Rev. Lett.* **80**, 2801–2804 (1998).

- <sup>20</sup> W. C. Chen, T. R. Gentile, T. G. Walker, and E. Babcock, [Phys. Rev. A](#) **75**, 013416 (2007).
- <sup>21</sup> I. A. Nelson and T. G. Walker, [Phys. Rev. A](#) **65**, 012712 (2002).
- <sup>22</sup> I. C. Ruset, Ph.D. thesis, University of New Hampshire, 2005.
- <sup>23</sup> M. A. Rosenberry, J. P. Reyes, D. Tupa, and T. J. Gay, [Phys. Rev. A](#) **75**, 023401 (2007).
- <sup>24</sup> X. H. Liu, H. Luo, T. L. Qu, K. Y. Yang, and Z. C. Ding, [AIP Advances](#) **5**, 107119 (2015).
- <sup>25</sup> G. D. Cates, R. J. Fitzgerald, A. S. Barton, P. Bogorad, M. Gatzke, N. R. Newbury, and B. Saam, [Phys. Rev. A](#) **45**, 4631–4639 (1992).